Atmos. Chem. Phys. Discuss., 7, 13653–13697, 2007
www.atmos-chem-phys-discuss.net/7/13653/2007/
© Author(s) 2007. This work is licensed
under a Creative Commons License.

Atmospheric Chemistry and Physics Discussions

Global distribution of mean age of stratospheric air from MIPAS SF_6 measurements

G. P. Stiller[1], T. von Clarmann[1], M. Höpfner[1], N. Glatthor[1], U. Grabowski[1], S. Kellmann[1], A. Kleinert[1], A. Linden[1], M. Milz[1,*], T. Reddmann[1], T. Steck[1], H. Fischer[1], B. Funke[2], M. López-Puertas[2], and A. Engel[3]

[1]Forschungszentrum Karlsruhe and University of Karlsruhe, Institut für Meteorologie und Klimaforschung, Karlsruhe, Germany
[2]Instituto de Astrofísica de Andalucía CSIC, Granada, Spain
[3]Institut für Atmosphäre und Umwelt, J. W. Goethe Universität Frankfurt am Main, Frankfurt, Germany
[*]now at: Institutionen för Rymdvetenskap, Luleå Tekniska Universitet, Kiruna, Sweden

Received: 27 July 2007 – Accepted: 10 September 2007 – Published: 18 September 2007

Correspondence to: G. P. Stiller (gabriele.stiller@imk.fzk.de)

Abstract

Global distributions of profiles of sulphur hexafluoride (SF_6) have been retrieved from limb emission spectra recorded by the Michelson Interferometer for Passive Atmospheric Sounding (MIPAS) on Envisat covering the period September 2002 to March 2004. Individual SF_6 profiles have a precision of 0.5 pptv below 25 km altitude and a vertical resolution of 4–6 km up to 35 km altitude. These data have been validated versus in situ observations obtained during balloon flights of a cryogenic whole-air sampler. For the tropical troposphere a trend of 0.227±0.008 pptv/yr has been derived from the MIPAS data, which is in excellent agreement with the trend from ground-based flask and in situ measurements from the National Oceanic and Atmospheric Administration Earth System Research Laboratory, Global Monitoring Division. For the data set currently available, based on at least three days of data per month, monthly 5° latitude mean values have a 1σ standard error of 1%. From the global SF_6 distributions, global daily and monthly distributions of the apparent mean age of air are inferred by application of the tropical tropospheric trend derived from MIPAS data. The inferred mean ages are provided for the full globe up to 90° N/S, and have a 1σ standard error of 0.25 yr. They range between 0 (near the tropical tropopause) and 7 years (except for situations of mesospheric intrusions) and agree well with earlier observations. The seasonal variation of the mean age of stratospheric air indicates episodes of severe intrusion of mesospheric air during each Northern and Southern polar winter observed, long-lasting remnants of old, subsided polar winter air over the spring and summer poles, and a rather short period of mixing with midlatitude air and/or upward transport during fall in October/November (NH) and April/May (SH), respectively, with small latitudinal gradients, immediately before the new polar vortex starts to form. The mean age distributions further confirm that SF_6 is destroyed in the mesosphere to a considerable amount. Model calculations with the Karlsruhe simulation model of the middle atmosphere (KASIMA) chemical transport model agree well with observed global distributions of the mean age only if the SF_6 sink reactions in the mesosphere are included

in the model.

1 Introduction

According to model predictions, climate change is expected to intensify the Brewer-Dobson circulation e.g. (Butchart et al., 2006; Austin and Li, 2006). This would mean that stratospheric air will become younger within a global warming scenario, providing feedback to stratospheric chemistry, e.g. the chlorine load (Waugh et al., 2007; Waugh and Hall, 2002). A measure of the transport time of an air parcel travelling from the tropopause to a certain location in the stratosphere is the so-called age of stratospheric air (Kida, 1983; Waugh and Hall, 2002). Due to mixing, an air parcel consists of air of different ages, characterized by its age spectrum (Waugh and Hall, 2002). The average over the age distribution is known as the mean age of stratospheric air, Γ. Austin and Li (2006) have demonstrated that the mean age of stratospheric air is a suitable measure for the intensity of the Brewer-Dobson circulation or the upwelling flux. The mean age of air is lowest near the tropical tropopause and increases both with latitude and altitude (Waugh and Hall, 2002), reflecting the respective travelling times in the global circulation. The mean age of stratospheric air can be derived from trace species which are stable within the troposphere and stratosphere and have a considerable trend which is, in the ideal case, linear. One suitable tracer for the measurement of the mean age of stratospheric air is sulphur hexafluoride (SF_6). It is produced almost entirely anthropogenically (Ko et al., 1993), has a well documented tropospheric increase that has been linear for the last 10 to 15 years (Geller et al., 1997), and is chemically inert in the troposphere and stratosphere. The only sinks to be considered are photolysis and electron capture reactions in the mesosphere (Morris et al., 1995; Ravishankara et al., 1993; Reddmann et al., 2001) leading to atmospheric lifetimes of several hundreds to thousands of years (Ravishankara et al., 1993; Morris et al., 1995). The mean age of air derived from SF_6 is generally in good agreement with that inferred from other tracers except in the polar vortices where intrusions of SF_6-depleted mesospheric air may play a role (Waugh and Hall, 2002). The mean age of air derived from SF_6 and not corrected for the mesospheric loss is sometimes referred to as the "apparent" mean age; whenever in this paper mean age of air derived from measured SF_6 is mentioned, the apparent mean age is meant.

Measurements of SF_6 and the mean age, in particular in the stratosphere, have been rather sparse until now. Long-term surface in situ and flask measurements from numerous sites are provided by the National Oceanic and Atmospheric Administration (NOAA) Earth System Research Laboratory (ESRL), Global Monitoring Division (GMD) via ftp://ftp.cmdl.noaa.gov/hats/sf6/. An airborne data set measured during various NASA ER-2 flights during the period 1992–1997 provided the most comprehensive stratospheric data set for Γ derived from CO_2 and SF_6 observations covering all latitudes between 85° N and 60° S, but only at one altitude (Boering et al., 1996; Elkins et al., 1996). Besides these observations, few vertical profiles from balloon-borne and airborne in situ and cryosampler instruments exist (Andrews et al., 2001; Strunk et al., 2000; Ray et al., 1999, 2002; Volk et al., 1997; Engel et al., 2006a,b). A few spectroscopic measurements of SF_6 in the infrared have been performed from the ground (Zander et al., 1991; Rinsland et al., 2003) and from the space-borne instruments ATMOS on the Space Shuttle (Rinsland et al., 1990; Zander et al., 1992; Rinsland et al., 1993) and ACE-FTS on SCISAT (Rinsland et al., 2005).

Recently Burgess et al. (2004, 2006) provided first global datasets of SF_6 from Michelson Interferometer for Passive Atmospheric Sounding/Environmental satellite (MIPAS/Envisat) spectral observations. They used MIPAS spectral data versions 4.53 to 4.59 (so-called "near-real time (NRT)" spectral data) for their analyses. The SF_6 global distributions revealed the main expected features, however, they were biased low by approximately 0.4 pptv compared to the NOAA/ESRL/GMD surface flask measurements. To our knowledge, no attempt has been made to derive the mean age of stratospheric air from this data set so far.

In this paper, we present an alternative approach to retrieve SF_6 from MIPAS/Envisat spectral data. Our data analysis is based on MIPAS high resolution spectra (ESA data version 4.61/62, so-called "re-processed" spectra) obtained from September 2002 to March 2004. After the description of the retrieval approach and the data characterization in terms of vertical resolution and error budget, global distributions of SF_6 are presented and their seasonal variation is discussed. We validate individual profiles by comparison to balloon-borne in situ observations. The tropical tropospheric trend is derived and compared to NOAA/ESRL/GMD surface in situ and flask measurements. The trend derived from the MIPAS measurements has been applied to infer the global distribution of mean age of stratospheric air, Γ. These data are compared to earlier observations, and their variability with time, altitude and latitude is analysed. Finally we address the importance of the mesospheric sink for age of air assessments from SF_6.

2 MIPAS

The Michelson Interferometer for Passive Atmospheric Sounding (MIPAS) is a mid-infrared Fourier transform limb emission spectrometer designed and operated for measurement of atmospheric trace species (Fischer et al., 2007). Its spectral resolution in its original measurement mode was 0.035 cm^{-1}, corresponding to an effective spectral resolution of 0.05 cm^{-1} after numerical apodization with the Norton Beer "strong" apodization function (Norton and Beer, 1976). It operated in this mode from March 2002 to March 2004. MIPAS is operated on the Envisat polar orbiting satellite and records a rear-viewing limb sequence of 17 spectra each 90 s, corresponding to an along track sampling of approximately 500 km and providing about 1000 vertical profiles per day along 14 orbits in its original observation mode. The vertical tangent altitude spacing is 3 km between 6 km and 42 km, which is the altitude range relevant to this study. The raw signal is processed by the European Space Agency (ESA) to produce calibrated geolocated limb emission spectra, labelled level 1-B data (Nett et al., 1999). After an instrument failure in March 2004, MIPAS resumed operation in a reduced spectral resolution mode with a variety of scan patterns providing

ACPD
7, 13653–13697, 2007

different altitude coverage, horizontal and vertical sampling. For this study, level 1-B version 4.61/62 data (so-called "reprocessed" data) from September 2002 to March 2004 have been used.

3 SF_6 Retrieval

3.1 Retrieval strategy

Retrievals presented here were carried out with the scientific MIPAS level 2 processor developed and operated by the Institute of Meteorology and Climate Research (IMK) in Karlsruhe together with the Instituto de Astrofísica de Andalucía (IAA) in Granada. The general retrieval strategy, which is a constrained multi-parameter non-linear least squares fitting of measured and modelled spectra, is described in detail in von Clarmann et al. (2003a,b). For radiative transfer modelling, the Karlsruhe Optimized and Precise Radiative Transfer model (KOPRA) (Stiller et al., 2002) has been used. Only aspects of specific interest in the context of the retrieval of SF_6 are discussed here.

The most suitable SF_6 signature in the mid infrared spectrum is the Q-branch of the ν_3 band at 947.9 cm^{-1}. The suitability of this band was first demonstrated by Rinsland et al. (1990). Also, all space-borne measurements of SF_6 that we are aware of rely on this band (ATMOS, ACE-FTS). In particular, Burgess et al. (2004, 2006) used spectral ranges from 929 to 931 cm^{-1} and 940 to 952 cm^{-1} for their SF_6 retrievals from MIPAS/Envisat. The main interfering species are CO_2, H_2O, and NH_3. The peak of the SF_6 signature is located at the near wing of the CO_2 fundamental band (FB; 00011 → 10001) laser line at 947.74 cm^{-1} and just above the first hot band (FH; 01111 → 11101) laser line at 947.94 cm^{-1}. Spectroscopic data from the dedicated MIPAS data base (Flaud et al., 2003) which is largely identical to the HITRAN 2004 data base (Rothman et al., 2005) has been used. In particular, temperature- and pressure-dependent SF_6 absorption cross sections for the spectral range 925 to 955 cm^{-1} and covering the atmospheric conditions of 180 to 295 K and 20 to 760 torr as provided by Varanasi et al. (1994) have been applied. It turned out that modelling of the line shapes of the interfering lines is extremely important for correct SF_6 retrievals. For this reason, several actions have been taken to improve the modelling of the spectral vicinity of the SF_6 band and these will be described in the following pragraphs.

Scattering of tropospheric radiance into the MIPAS line of sight by cloud particles was shown by Höpfner et al. (2002) to have a considerable effect on the spectral line shapes, particularly in the spectral region relevant to the SF_6 retrieval. For this reason, specific care has been taken to exclude all spectra of particle-contaminated scenes from the data analysis. Rejection of cloud/aerosol contaminated MIPAS spectra was performed according to the colour ratio method of Spang et al. (2004) who used the ratio of the spectral regions 788.2–796.25 cm^{-1} and 832.3–834.4 cm^{-1}, the so-called cloud index CI, to detect a cloud/aerosol signal in the spectra. In our study, a very rigorous cloud index of 6, which reliably excludes any spectra contaminated by cloud signal (Glatthor et al., 2006), has been applied (i.e. all spectra having a cloud index of 6 or lower have been excluded from the retrievals).

Prior to the retrieval of SF_6 volume mixing ratios (vmrs), the following quantities were retrieved and the resulting profiles were used as a priori information in the SF_6 retrievals: residual spectral shift, instrument line shape correction, temperature and line of sight (von Clarmann et al., 2003b), and ozone. NH_3 and COF_2 emissions were also considered in the radiative transfer modelling, using climatological profiles for these trace species. The spectral range used for SF_6 retrieval was 945.4 cm^{-1} to 948.5 cm^{-1} (see Fig. 1). Simultaneously with SF_6, CO_2 and H_2O vmrs were retrieved in a multi-parameter retrieval approach. Beyond this, the background continuum emission and zero radiance calibration correction were retrieved jointly. The rationale of this approach is discussed in detail in von Clarmann et al. (2003b).

In the vicinity of the SF_6 signatures non-local thermodynamic equilibrium (non-LTE) effects are an important issue for the CO_2 lines (López-Puertas and Taylor, 2001). To correct for these non-LTE emissions, but to keep the computational effort reasonably low, the CO_2 lines of the FB and the FH laser band, respectively, have been modelled in a first-order approach by retrieving a CO_2 pseudo-vmr, i.e. a volume mixing ratio which, under LTE assumption, causes the same emission as the true CO_2 vmr under non-LTE. Since the two relevant bands are differently affected by non-LTE effects, the lines of the two bands were handled formally as if they belonged to different trace species. In order to constrain the CO_2 line of the FH laser band just below the SF_6 signature, further lines of the same band near 945.4 cm^{-1}, 946.7 cm^{-1}, and 947.1 cm^{-1} were also fitted. An example of measured and best-fit spectra, together with the assignment of the trace species spectral signatures is shown in Fig. 1. Due to non-linearity effects in radiative transfer, adjusting the pseudo-vmr to fit a spectral line instead of adjusting the non-LTE vibrational populations of the molecular states is only an approximation. The systematic errors introduced by this approach are discussed in Sect. 3.2.

The retrieval is performed on an altitude grid of 1 km step widths up to 44 km and 2–20 km steps above, and is regularized by a Tikhonov-type constraint which adds to the objective function of the least squares fit a penalty which keeps the differences of mixing ratios at adjacent altitudes reasonably small (Tikhonov, 1963; Steck and von Clarmann, 2001; Steck, 2002). This is achieved by using a smoothness constraint matrix of the type $\gamma \mathbf{L}_1^T \mathbf{L}_1$ where γ is a scaling factor and $\mathbf{L}_1$ is a first order finite differences operator. The use of the latter does not constrain the column information but only how this information is distributed over altitude and, thus, provides a bias-free retrieval. A typical profile is presented in Fig. 2, upper panel, together with its uncertainties due to measurement noise. The regularization strength has been adjusted such that about 4 degrees of freedom are obtained within the altitude range 8–35 km, resulting in a vertical resolution of 4 km near the tropopause and 8 km above 35 km (see Fig. 2, middle panel). In order not to introduce any artefacts in the profile structure, an all-zero flat a priori profile has been used.

Error estimation is based on linear theory as suggested by Rodgers (2000). The error budget of the profile in Fig. 2 is provided in the third panel. The error budget includes the mapping of the measurement noise on the retrieved volume mixing ratios as well as the propagation of uncertainties of model parameters onto the result. Up to approximately 25 km, the total uncertainty in the SF_6 vmr profiles is 0.4 to 0.5 pptv (9 to 17%), with the measurement noise as the dominating error source.

Further contributing model parameter errors are the errors due to the uncertainties in temperature (tem), line-of-sight (los) (from preceding retrievals), NH_3 (nh3) (from climatological variability), horizontal temperature gradients (tgra), residual uncertainties in radiance (gain) and frequency shift calibration (shift), and residual uncertainties in the instrumental line shape (ils). Other model parameter errors were found to be negligible. The main model parameter error contributions, however also of random nature, are the uncertainties due to the interference of NH_3 lines for which the atmospheric volume mixing ratio is unknown, and the residual line-of-sight uncertainty. The only non-negligible systematic error source besides the spectroscopic uncertainty (reported to be a few percent Nemtchinov and Varanasi, 2003), is the residual instrumental line shape uncertainty which contributes with approximately 5% (0.2 to 0.3 pptv) to the over-all error budget above 30 km. Typically, we use data sets from at least three observational days representing one month of measurements to construct zonal mean distributions which provide, for 5° latitude bins, roughly 100 observations per bin, reducing the SF_6 standard error of the mean to 1%.

The error estimation does not include the smoothing error, nor the mapping of the smoothing error of joint fit parameters onto the SF_6 profile, since both of these errors require robust knowledge of the true covariance matrices of these species (Rodgers, 2000), which is, to our judgment, not available.

3.2 Consideration of non-LTE emissions for interfering CO_2 lines

As described above, the handling of differing non-LTE effects for lines from different spectroscopic bands has been treated by a simplified approach. In order to assess the systematic error potentially introduced by this approach, a limited data set (covering two days in November 2003 and January 2004) was treated with a non-LTE approach for the CO_2 FB and FH laser band lines using pre-calculated populations of the respective CO_2 molecular states. These have been derived within the preceding retrieval of CO for the respective days, since the CO retrieval requires full CO_2 non-LTE modelling (Funke et al., 2007), using the GRANADA non-LTE model (Funke et al., 2001).

The non-LTE emissions of the CO_2 lines then were modelled by making use of the non-LTE functionality of the radiative transfer model KOPRA (Stiller et al., 2002) implemented in the scientific IMK/IAA MIPAS data processor.

Comparison of the simplified approach with the full non-LTE treatment (see Fig. 3) reveals systematic differences for both days in terms of a high bias of the simplified approach (0 to 0.1 pptv or 0 to +2%) between 10 and 20 km (tropics) and 15 and 25 km (high latitudes) and a low bias (0 to 0.2 pptv or 0 to 4%) at 25 to 35 km altitude. The low bias is most pronounced, with values of 0.5 pptv or higher, above 35 km over the summer pole due to the prevailing illumination, keeping in mind that the CO_2 non-LTE effects are mainly due to solar excitation.

This means that inferred mean age of air (on the basis of a trend of 0.22 pptv yr^{-1}) is expected to be 0 to 0.5 years too low in the lower stratosphere and 0 to 1 year too high above 25 km; a maximum bias of up to 2 years is reached at the summer pole above 35 km only, an altitude range which is not used in this study for the assessment of the mean age of air. Since this effect, although of systematic nature, has no simple altitude and latitude relationship, we have not corrected the data set and use original uncorrected data for our study. Re-processing of the complete data set in order to eliminate the bias was not possible at this time due to missing CO_2 vibrational temperatures (provided from CO retrievals) for most of the days included in this analysis.

3.3 Effects and handling of imperfect gain calibration

Peculiar high day-to-day variability in global SF_6 distributions provided another hint towards a systematic error in the data. It turned out that the SF_6 retrievals were extremely sensitive to very small systematic oscillations in the radiance baseline, affecting the shape of the SF_6 signature itself and that of interfering lines. These baseline oscillations are well below the NESR (Noise Equivalent Spectral Radiance) specification of MIPAS and become visible only after averaging a huge number of spectra. Nevertheless, the SF_6 retrievals, at least above 20 to 25 km, are systematically affected by these oscillations, which occur in the version 4.61 and 4.62 spectra only. These radiance baseline oscillations are of different nature than the gain error listed in the error budget (see Fig. 2). The latter is the uncertainty of the scaling of the spectrum. A method to quantify the systematic contribution to the SF_6 retrievals and to correct the SF_6 distributions for this contribution has been developed and applied to the data set presented in this study. Technical details about the correction method are given in the Appendix.

4 Comparison to balloon-borne cryo-sampler data

During the first observation phase of MIPAS from July 2002 to March 2004 several field campaigns took place, some of them intended for validation of Envisat instruments. The balloon-borne cryogenic whole-air sampler BONBON (Engel et al., 2006b) which provides highly accurate data, measured during three balloon flights, one on 24 September 2002 in Southern France, the other two on 6 March 2003 and 9 June 2003 near Kiruna, North Sweden. Figure 4 presents the comparison of co-incident MIPAS profiles with the in situ data, together with a map showing the locations, the temporal and spatial mis-matches and the potential vorticity (PV) fields. For good co-incidences, the MIPAS profiles agree with the BONBON data to within 0.5 pptv below 25 km which is fully consistent with the estimated error budget. For 24 September 2002, the bias-corrected profiles are also shown; the bias for this day is one of the smaller ones, but not negligible.

5 Global SF_6 distributions

Global distributions of SF_6 on basis of bias-corrected data have been derived for the period September 2002 to March 2004 for at least 3 days per month. Figure 5 provides as an example the 5° zonally averaged global distribution for March 2003. For each 5° latitude bin, approximately 140 individual profiles have been averaged, leading to a mean value standard error in the order of 0.05 pptv or 1%. The zonal mean distribution reveals all features expected from earlier observations: Tropospheric SF_6 is homogeneously distributed with values between 5.0 and 5.5 pptv, but slightly higher in the Northern hemisphere due to industrial sources. The SF_6 vmr is decreasing both with altitude and latitude, reflecting the travelling time needed to transport air parcels from the tropical tropopause to higher altitudes and latitudes. The stratospheric SF_6 vmr over the spring pole is lowest since the aged polar vortex is filled with old air which might also have experienced SF_6 depletion in the mesosphere. Figure 6 provides the seasonal and latitudinal variation of SF_6 monthly zonal profiles (averaged for 5° latitude bins). The seasonal variation is very small in the tropics and most pronounced at high latitudes.

6 Tropical tropospheric SF_6 trend

The tropical tropospheric trend of MIPAS SF_6 observations was derived from daily mean values averaged over 17.5°S to 17.5°N and 9 to 15 km (Fig. 7). The linear regression provides a trend of 0.227±0.008 pptv/year with an extrapolated value of 4.89 pptv on 1 January 2002. This is in excellent agreement with globally averaged ground-based flask and in situ observations as provided by the National Oceanic and Atmospheric Administration/Earth System Research Laboratory, Global Monitoring Division in Boulder, CO (data from ftp://ftp.cmdl.noaa.gov/hats/sf6/insituGCs/CATS/global/insitu_global_SF6 and ftp://ftp.cmdl.noaa.gov/hats/sf6/flasks/sf6global.txt): The trend reported for NOAA/ESRL/GMD in situ global data is 0.224±0.002 pptv/year, and for flask data it is 0.217±0.003 pptv/year; both data sets provide a global mean of 4.88±0.03 pptv in January 2002 (B. Hall, personal communication, 2007). The mean age of stratospheric air can be inferred from stratospheric SF_6 distributions as the time lag since the troposphere showed the mixing ratio measured in the stratosphere, if the tropospheric trend is well known and linear (if not linear, the mean age will not represent the age spectrum of the air parcel). The MIPAS-derived trend has been used to convert SF_6 global distributions into mean age of stratospheric air, assuming that the trend has remained linear and constant within the relevant period. This indeed is confirmed by the NOAA/ESRL/GMD measurements.

7 Mean age of stratospheric air

7.1 Global distributions

The global distribution of the mean age of stratospheric air derived from MIPAS SF_6 monthly zonal means (provided for potential temperature versus equivalent latitudes) is shown in Fig. 8 for the months September 2002, December 2002, March 2003, and June 2003. While ascent of young air is most pronounced over the tropics during the Northern hemispheric summer months (Fig. 8, bottom right panel), very old air is found for all polar winter vortices (top and bottom right panels). During fall (top and bottom left panels) in the respective hemisphere, the horizontal age gradients in the middle stratosphere are lowest, providing nearly mid-latitudinal conditions in the polar regions. During spring (top and bottom left panels) the surf zone in mid latitudes is most pronounced revealing latitudinally nearly constant mean age of air in the lower to middle stratosphere, which is produced by isentropic mixing due to planetary waves.

The surf zone is separated from the tropics, and even more sharply separated from the polar vortex, by a barrier revealing very high horizontal age gradients. Also remarkable is the remnant of old air in the middle stratospheric Austral summer above 850 K during December 2002 (Fig. 8, top right panel).

A compilation of monthly zonally averaged age of air distributions at three different altitudes is shown in Fig. 9. In the tropics and mid-latitudes, the seasonal and interannual variation over the 19 months covered by our data is rather low. Similar figures are available from, e.g. NASA ER-2 observations of the mean age of air (see, for example, Waugh and Hall, 2002, their Fig. 6); the MIPAS results can be compared directly with those and provide, additionally, data for the Southern hemisphere polar region. For 20 km altitude, the tropical mean age of air from MIPAS is between 0.5 and 2.5 years while the ER-2 observations yield an age around 1 year. The mean age increases with latitude for both hemispheres, with a significant seasonal variation in the polar regions. During polar winter on the Northern hemisphere, the highest MIPAS values are around 6 years, while near the South pole, the spread is considerably larger with SF_6-derived apparent a ges of up to 9.5 years in winter and spring. From the ER-2 data set, Northern hemispheric ages of up to 6 years, and 60°S ages up to 5.5 years were derived, which are consistent with our data set. The inter-annual variation is also remarkable (compare, for instance, September 2002 to September 2003). During September 2002 an unprecedented Southern hemispheric major warming took place, with very high planetary wave activity (Manney et al., 2005b) which might be reflected in the slightly unusual age of air distribution. For 16 km altitude (first panel of Fig. 9), i.e. just at the altitude of the tropical tropopause layer, the age of air in the tropics is between 0 and 1.5 years, as expected. For polar regions, ages between 2 and 5 years in the North and 3 to 7 years in the South are observed. For higher altitudes (e.g. 25 km, third panel of Fig. 9) the tropical mean age of air is around 3 to 3.5 years, while the seasonality and inter-annual variation at the poles becomes even more pronounced, suggesting increasing impact of mesospheric intrusions (see below).

Figure 10 presents zonally averaged (5°latitude bins) monthly mean profiles for several latitudes and months, similar to Waugh and Hall (2002), their Fig. 6. The age of air is lowest for the tropical latitude bin and highest for the latitude bin near the South pole. The variation with altitude and season is most pronounced for the polar latitudes. In particular for higher altitudes, the MIPAS ages seem to have a slight tendency to higher values than the observations presented by Waugh and Hall (2002), although the variability in MIPAS data covers the previous observations in all cases. The systematic high bias in the present MIPAS age data set due to the CO_2 non-LTE treatment, which can potentially reach 1 year for altitudes above 25 km (see Sect. 3.2 and Fig. 3) should be kept in mind for these comparisons.

7.2 Temporal variation

The seasonal variation and inter-annual differences are most clearly displayed by time series of equivalent-latitude distributions at certain potential temperature levels (see Fig. 11) and those of vertical profiles (in terms of potential temperature as vertical coordinate) for certain equivalent-latitude bands (see Fig. 12). During Austral winter, extremely high apparent ages of 12 years or more, in fact unrealistic high, were observed at the 625 K surface and above (see Fig. 11, top panel, and Fig. 12, bottom panel) during two episodes (June to July 2003; September to November 2003), separated by an episode of younger air (August 2003). The first episode of high mean age started rather abruptly in June 2003; in July the polar vortex was filled with air older than 8 years, south of 70° S equivalent latitude for altitudes above the 575 K potential temperature level. After the break in August 2003, the latitude- and altitude regime filled up with old air even increased; this situation lasted until end of November. The Antarctic winter 2003 has been characterized from observations of CO (Funke et al., 2005) and NO_x (Funke et al., 2005; Randall et al., 2007) by a very strong vortex with long-lasting and severe transport of mesospheric air into the stratospheric vortex. Hence, the very high apparent age of air observed is most probably due to SF_6-depleted mesospheric air masses filling the stratospheric vortex. In contrast to the very long-lasting area of old air masses in 2003, the very old air disappeared earlier in 2002, probably due to the weak vortex being perturbed frequently by planetary wave activity which finally led to the first observed Southern Hemispheric major warming (Manney et al., 2005b). Although very high ages were no longer observed during Southern summer, the mean age of air remained rather high even then, with values around 6 to 8 years. Only im-

ACPD

7, 13653–13697, 2007

Global mean age of air from MIPAS

G. P. Stiller et al.

EGU

mediately before the formation of the next polar vortex, in April/May, ages closer to mid-latitude conditions were observed at high Southern latitudes, indicating that polar summer air was mixed with lower-latitude air.

The Northern hemispheric winter is rather different than the Southern hemispheric one since obvious subsidence episodes are shorter, and the high ages of the Southern hemispheric winter have not been observed (Fig. 11 and Fig. 12, top panel). The highest age of air observed at 625 K during the measurement time of MIPAS is 8 to 9 years, in March 2003 and 2004. The early winter 2002 (December 2002) was outstanding due to heavy intrusions of mesospheric air into the polar vortex (Konopka et al., 2007; Engel et al., 2006b). This is confirmed by MIPAS age of air observations. However, although the 8-year isoline came down to about 675 K in December 2002, the mesospheric intrusion did obviously not last long enough to fill up the vortex with aged mesospheric air. Another extreme winter was the late winter 2004 (Manney et al., 2005a; Randall et al., 2006). During January to March 2004, strong subsidence of upper atmospheric NO_x into the polar stratosphere has been observed by various instruments (Randall et al., 2006; Seppälä et al., 2007; Hauchecorne et al., 2007; Funke et al., 2007[1]). This again is confirmed by the observed age of air, since ages of 8 years and more have been observed above 600 K. However, it is obvious that, despite severe subsidence events, similar high ages of air as for the Southern hemispheric winter 2003 are unusual for Northern hemispheric winters; at least air of comparable age has not been observed during the two Northern hemispheric winters covered by MIPAS (see Fig. 11). Considerable inter-hemispheric differences are also observed at high latitudes at the 400 K level (see Fig. 11, lower panel), with air again being much older in the Southern hemisphere.

The age of air in the tropics at 400 K is rather constant over the seasons, except that a slight seasonal oscillation with latitudes can be observed. At 625 K and above (see

[1]Funke, B., Lòpez-Puertas, L., Stiller, G., von Clarmann, T., Grabowski, U., and Linden, A.: Upper atmospheric NO_x intrusions into the Arctic stratospshere during January–April 2004, to be submitted, Atmos. Chem. Phys. Discuss., 2007.

ACPD

7, 13653–13697, 2007

Fig. 11 and Fig. 12, second panel) the mean age of air seems to increase with time. Indications for a quasiperiodic variation of the stratospheric mean age were already found by Schmidt and Khedim (1991) who analysed a time series of CO_2-derived age measurements in the Northern hemisphere covering the period 1975 to 1990. We assume that the tropical variation in the MIPAS data set is linked to the quasi-biennial oscillation (QBO) which changed phases around June 2003; a detailed analysis is under investigation.

7.3 Comparison to model calculations

Observations of apparent age of air derived from SF_6 vmrs of more than 6 to 8 years were also reported previously (Engel et al., 2006b; Hall and Waugh, 1998; Waugh and Hall, 2002). However, other age of air tracers like CO_2 do not confirm these high ages; the mesospheric loss of SF_6 is generally considered to explain this discrepancy (Hall and Waugh, 1998; Reddmann et al., 2001). In order to confirm that the high mean age values derived from MIPAS observations during polar winters can be explained by the mesospheric sink of SF_6, w e performed model simulations with the Karlsruhe simulation model of the middle atmosphere (KASIMA), a 3D-chemistry transport model which includes a module for SF_6 chemistry in the mesosphere (Reddmann et al., 2001). SF_6 is mainly destroyed via electron attachment and subsequent transformation to HF.

For the present studies, the model version as described in Reddmann et al. (2001) is applied, but using ERA-40 analyses up to 18 km, a relaxation term up to 1 hPa and the prognostic part of the model above. From the lower pressure height boundary at 7 km up to 22 km, the vertical resolution is 750 m. From 22 km up to the upper boundary at 120 km, the vertical spacing between the levels gradually increases to 3.8 km. The triangular truncation, T21, used corresponds to a horizontal resolution of about $5.7^{\circ}\times5.7^{\circ}$. A numerical time step of 12 min was used in the experiments.

As described in Reddmann et al. (2001) assumptions on the free thermal electron density and the reaction constants used influence the results. Here we use a ionisation model and include all back reactions, corresponding to an atmospheric lifetime of about 4500 years.

Figure 13 compares the monthly global mean distribution of MIPAS age of air for October 2003 (top panel) with KASIMA calculations including (middle panel) or disregarding (bottom panel) the mesospheric sink reaction. In the first case, the apparent ages produced over the South pole are much closer to the MIPAS observations. In fact, the age of air calculated from this model run is 12 years or more, in very good agreement with the MIPAS observations. In contrast, treating SF_6 as a fully stable tracer produces ages around 6 to 8 years over the South pole which has to be considered as the real transport time. This comparison confirms the assumption that high apparent ages as derived from SF_6 are due to transport of SF_6-depleted mesospheric air into the stratosphere.

The MIPAS time series show that such mesospheric intrusions are quite a frequent phenomenon. Further, the comparison roughly confirms the atmospheric lifetime of SF_6 assessed by this study to be about 4500 years. Finally, the importance of the mesospheric SF_6 sink is emphasized when comparing chemistry-transport models with age of air data derived from SF_6. A more detailed analysis of the MIPAS data set together with model simulations of the global mean age of air distribution is planned for the near future.

8 Conclusions

We have derived mean age of air global distributions for the altitude range 6 to 35 km and the period September 2002 to March 2004 from MIPAS/Envisat SF_6 observations with a precision (in terms of the standard error of monthly 5° zonal means based on approximately 100 single observations each) of 0.25 yr. The systematic error of the mean age of air data set is ruled by the uncertainty in spectroscopic data and a simplified non-LTE treatment in the SF_6 retrieval approach which both might explain a potential bias of up to 1 year for certain altitudes, latitudes, and seasons. Comparison to previous observations reveals that the SF_6 and mean age of air distributions from MIPAS are in very good agreement with those which indicates that the actual systematic error is considerably lower than its estimate. The available age of air data set gives the unprecedented opportunity to validate the transport schemes in chemistry-transport and chemistry-climate models.

The global data set from MIPAS for the period September 2002 to March 2004 reveals high seasonal and inter-annual variability and pronounced inter-hemispheric differences. In particular, in both polar vortices, frequent and, for the Southern hemisphere, long-lasting intrusions of mesospheric air into the stratospheric vortex are observed, identified by very high apparent mean ages of 8 to 12 years and higher. The frequent mesospheric intrusions seen in MIPAS data may have been underestimated in the past and their role on chemistry-climate coupling needs further assessment. The mesospheric depletion of SF_6 has been confirmed as source of the overestimation of the mean age of air by comparison of the observations with model calculations including and disregarding, respectively, the mesospheric chemical sink reactions of SF_6. Since MIPAS data contain independent information to quantify subsidence of mesospheric air (via CO or CH_4, cf. Funke et al., 2005), the mesospheric sink strength, which is coupled to the mesospheric electron density, can be unambiguously quantified. This will help to improve the age of air assessment from SF_6 and to make it more consistent with age of air estimates based on other tracers. Beyond these polar-winter related issues, the potential role of the quasi-biennial oscillation (QBO) in the temporal variation of the measured tropical mean age of air distribution as suggested above still needs to be confirmed.

SF_6 distributions discussed in this paper were retrieved from MIPAS high resolution spectra recorded in the original measurement mode before an instrument failure forced spectral degradation. For the assessment of a trend in the Brewer-Dobson circulation, an extended time series is necessary. This is because the high seasonal and inter-annual variability observed is an obstacle to the unambiguous detection of a change in middle atmospheric global circulation from the currently available data set. However, 5 years of MIPAS level 1-B data are now available, and an extension of the mission for

ACPD
7, 13653–13697, 2007

another 3 to 7 years is planned. This will provide a tremendous amount of information, assuming an equally accurate SF_6 retrieval will be possible from the reduced-resolution spectral data, which still has to be proven.

Appendix A

Correction of SF_6 vmr biases caused by inadequate gain calibration

The original MIPAS time series of SF_6 is characterized by occasional unphysical values, which form secondary modes in the histogram of SF_6 daily mean values. In order to reject or correct unrealistic values from the assessment of the age of the air without running risk of rejecting/correcting any true but unexpected data caused by unknown chemistry or physics, a search was made for an external data filter which is independent of the SF_6 values themselves. Since discontinuities in SF_6 mixing ratios were found to coincide exactly with the changes of the MIPAS gain calibration function, it was necessary to further assess the MIPAS calibration characteristics in the SF_6 microwindow. MIPAS radiance calibration is done by application of one gain calibration function over a period of typically several days. For all limb sequences within such a gain calibration period, the spectra of the uppermost tangent altitude (approximately 68 km) were averaged over time. This was done separately for spectra recorded during forward and backward movement of the interferometer mirrors, because calibration is done separately for forward and backward measurements.

Since, except for the two CO_2 FB laser band lines, all other atmospheric signals (e.g. CO_2 laser hot band lines, CO_2 isotope transitions, H_2O, SF_6) are too weak to be noticeable, zero signal is expected in the gaps between the two prominent CO_2 lines in the averaged spectra. Instead, for several gain calibration periods, systematic deviations from the zero radiance level were observed (see Fig. 14). The amplitude of this error in the calibrated spectra is below the NESR of a single spectrum, and within the MIPAS radiance calibration specifications, but clearly visible in the averaged spectra.

Since the gain calibration functions are applied multiplicatively, it is not quite obvious how zero radiances can be affected and one might tend to attribute this artefact to the (additive) offset calibration function. The latter, however, is updated several times per orbit and does not coincide with the changes of the observed artefact. Thus, the nature of the detected artefact is still unexplained; since the details of the implementation of the calibration algorithm are beyond our direct control, we restrict ourselves to correct the affected SF_6 vmr data.

In a transparent atmosphere where radiative transfer is linear, and when measurement noise is equidistributed within the spectral gridpoints under consideration, the mapping of a systematic measurement error on the retrieved target mixing ratio is proportional to the product of the row vector containing the typical target spectral signal and the column vector containing the spectral error. Thus we estimate the retrieval error due to baseline oscillations caused by inadequate radiance calibration, in arbitrary units, as

$$\Delta SF_6 = c \times \sum_{n=1}^{N} y_{SF_6;n} \times \left(y_{art.,fw;n} + y_{art.,bw;n} - \frac{\sum_{n=1}^{N} y_{art.,fw;n}}{N} - \frac{\sum_{n=1}^{N} y_{art.,bw;n}}{N}\right) \quad \text{(A1)}$$

where n runs over all N spectral gridpoints of the SF_6 microwindow except those where the prominent CO_2 laser band lines are situated. c is a constant of the dimension [pptv $(W/(cm^{-2}\,sr\,cm^{-1}))^{-2}$]; $y_{SF_6;n}$ is the spectral signal of the SF_6 band, and $y_{art.,fw;n}$ and $y_{art.,bw;n}$ are the systematic radiance errors at spectral gridpoint n in the forward and backward spectra, respectively. The subtraction of the average background signal accounts for the average offset correction in our retrieval (von Clarmann et al., 2003b). This ΔSF_6 value, further referred to as gain index, was used as measure of the impact of erroneous gain calibration in further correction steps. In total, 87 gain calibration periods were analyzed by means of the spectral analysis described above, all of them applied within the period September 2002 to end of March 2004, and 87 gain indices were derived.

For correction of the SF_6 vmrs distorted by imperfect radiance calibration, SF_6 global means (90° S–90° N) per orbit for all altitude levels for two height grids, from 44 km to 7 km and 1500 K to 350 K, were calculated. These orbit mean values for each altitude were correlated with the gain indices derived for the respective orbits. A linear relationship between orbit-mean SF_6 vmrs and gain indices was established for all altitudes and potential temperature levels (see Fig. 15). From the linear regression of this correlation an additive correction term for each altitude or potential temperature level was derived. For all daily and monthly mean distributions, each SF_6 value has been corrected by the following expression

$$SF_6^{korr}(z, \text{orbit}) = SF_6^{original}(z, \text{orbit}) - a(z) * \text{gain\_index}(\text{orbit}) \tag{A2}$$

with a(z) being the altitude dependent slope of the linear regression (SF_6 vs. gain index) (see Fig. 15) and gain_index(orbit) the orbit-dependent gain index characterizing the error due to inadequate gain calibration. a(z) is of the order of 1.0 for 44 km altitude and decreases smoothly to values around 0.06 for 10 km, while the gain index varies between −4.0 and +2.5 for the gain calibration periods under investigation. For SF_6 means built from more than one gain calibration periods, the weighted mean of the gain indices was applied.

It should be noted that the method described above could lead to an unwanted artificial component in the temporal variation of SF_6 in terms of seasonal variation or trend, if the gain index varied systematically with time as well. The latter, however, has been falsified, i.e. it was found that the gain index varied randomly with time rather than systematically.

Within this work, scientific analysis of SF_6 distributions, and, in particular, the derivation of the tropospheric trend and mean age of stratospheric air, is based on the corrected SF_6 data. Figure 16 presents the time series of global SF_6 at 25 km altitude before and after correction. In summary, while the correction is substantial, the expected SF_6 vmr values or any expected structures are never used in the correction scheme. Instead, the correction relies fully and solely on the detected gain calibration peculiarities.

Acknowledgements. Re-processed MIPAS level 1-B data were provided by ESA for scientific analysis. The research work of the IMK MIPAS/Envisat group has been funded by EC via the Integrated Project SCOUT-O3 (contract no. 505390-GOCE-CT-2004), BMBF via project No. 50EE0512, and the German Research Foundation (DFG) within the Program of Emphasis CAWSES via project STI 210/4-1. We gratefully acknowledge the provision of SF_6 surface flask and in situ measurements by the National Oceanic and Atmospheric Administration Earth System Research Laboratory, Global Monitoring Division, and helpful comments on the manuscript by B. Hall.

References

Andrews, A. E., Boering, K. A., Daube, B. C., Wofsy, S. C., Loewenstein, M., Jost, H., Podolske, J. R., Webster, C. R., Herman, R. L., Scott, D. C., Flesch, G. J., Moyer, E. J., Elkins, J. W., Dutton, G. S., Hurst, D. F., Moore, F. L., Ray, E. A., Romashkin, P. A., and Strahan, S. E.: Mean ages of stratospheric air derived from in situ observations of CO_2, CH_4, and N_2O, J. Geophys. Res., 106, 32 295–32 314, doi:10.1029/2001JD000465, 2001. 13656

Austin, J. and Li, F.: On the relationship between the strength of the Brewer-Dobson circulation and the age of stratospheric air, Geophys. Res. Lett., 33, L17807, doi:10.1029/2006GL026867, 2006. 13655

Boering, K. A., Wofsy, S. C., Daube, B. C., Schneider, H. R., Loewenstein, M., Podolske, J. R., and Conway, T. J.: Stratospheric Mean Ages and Transport Rates from Observations of Carbon Dioxide and Nitrous Oxide, Science, 274, 1340–1343, doi:10.1126/science.274.5291.1340, 1996. 13656

Burgess, A. B., Grainger, R. G., Dudhia, A., Payne, V. H., and Jay, V. L.: MIPAS measurement of sulphur hexafluoride (SF_6), Geophys. Res. Lett., 31, L05112, doi:10.1029/2003GL019143, 2004. 13656, 13658

Burgess, A. B., Grainger, R. G., and Dudhia, A.: Zonal mean atmospheric distribution of sulphur hexafluoride (SF_6), Geophys. Res. Lett., 33, L07809, doi:10.1029/2005GL025410, 2006. 13656, 13658

Butchart, N., Scaife, A. A., Bourqui, M., de Grandpre, J., Hare, S. H. E., Kettleborough, J., Langematz, U., Manzini, E., Sassi, F., Shibata, K., Shindell, D., and Sigmond, M.: Simulations of anthropogenic change in the strength of the Brewer-Dobson circulation, Clim. Dyn., 27, 727–741, doi:10.1007/s00382-006-0162-4, 2006. 13655

Elkins, J. W., Fahey, D. W., Gilligan, J. M., Dutton, G. S., Baring, T. J., Volk, C. M., Dunn, R. E., Myers, R. C., Montzka, S. A., Wamsley, P. R., Hayden, A. H., Butler, J. H., Thompson, T. M., Swanson, T. H., Dlugokencky, E. J., Novelli, P. C., Hurst, D. F., Lobert, J. M., Ciciora, S. J., McLaughlin, R. J., Thompson, T. L., Winkler, R. H., Fraser, P. J., Steele, L. P., and Lucarelli, M. P.: Airborne gas chromatograph for in situ measurements of long-lived species in the upper troposphere and lower stratosphere, Geophys. Res. Lett., 23, 347–350, doi:10.1029/96GL00244, 1996. 13656

Engel, A., Bönisch, H., Brunner, D., Fischer, H., Franke, H., Günther, G., Gurk, C., Hegglin, M., Hoor, P., Königstedt, R., Krebsbach, M., Maser, R., Parchatka, U., Peter, T., Schell, D., Schiller, C., Schmidt, U., Spelten, N., Szabo, T., Weers, U., Wernli, H., Wetter, T., and Wirth, V.: Highly resolved observations of trace gases in the lowermost stratosphere and upper troposphere from the Spurt project: an overview, Atmos. Chem. Phys., 6, 283–301, 2006a. 13656

Engel, A., Möbius, T., Haase, H.-P., Bönisch, H., Wetter, T., Schmidt, U., Levin, I., Reddmann, T., Oelhaf, H., Wetzel, G., Grunow, K., Huret, N., and Pirre, M.: Observation of mesospheric air inside the arctic stratospheric polar vortex in early 2003, Atmos. Chem. Phys., 6, 267–282, 2006b. 13656, 13663, 13668, 13669, 13685

Fischer, H., Birk, M., Blom, C., Carli, B., Carlotti, M., von Clarmann, T., Delbouille, L., Dudhia, A., Ehhalt, D., Endemann, M., Flaud, J. M., Gessner, R., Kleinert, A., Koopmann, R., Langen, J., López-Puertas, M., Mosner, P., Nett, H., Oelhaf, H., Perron, G., Remedios, J., Ridolfi, M., Stiller, G., and Zander, R.: MIPAS: an instrument for atmospheric and climate research, Atmos. Chem. Phys. Discuss., 7, 8795–8893, 2007, http://www.atmos-chem-phys-discuss.net/7/8795/2007/. 13657

Flaud, J.-M., Piccolo, C., Carli, B., Perrin, A., Coudert, L. H., Teffo, J.-L., and Brown, L. R.: Molecular line parameters for the MIPAS (Michelson Interferometer for Passive Atmospheric Sounding) experiment, Atmos. Oceanic Opt., 16, 172–182, 2003. 13658

Funke, B., López-Puertas, M., Stiller, G. P., von Clarmann, T., and Höpfner, M.: A new non–LTE Retrieval Method for Atmospheric Parameters From MIPAS–ENVISAT Emission Spectra, Adv. Space Res., 27, 1099–1104, 2001. 13662

Funke, B., López-Puertas, M., Gil-López, S., von Clarmann, T., Stiller, G. P., Fischer, H., and Kellmann, S.: Downward transport of upper atmospheric NO_x into the polar stratosphere and lower mesosphere during the Antarctic 2003 and Arctic 2002/2003 winters, J. Geophys. Res., 110, D24308, doi:10.1029/2005JD006463, 2005. 13667, 13671

Funke, B., López-Puertas, M., , Bermejo-Pantaleón, D., von Clarmann, T., Stiller, G. P., Höpfner, M., Grabowski, U., and Kaufmann, M.: Analysis of nonlocal thermodynamic equilibrium CO 4.7 μm fundamental, isotopic and hot band emissions measured by the Michelson Interferometer for Passive Atmospheric Sounding on Envisat, J. Geophys. Res., 112, D11305, doi:10.1029/2006JD007933, 2007. 13662

Geller, L. S., Elkins, J. W., Lobert, J. M., Clarke, A. D., Hurst, D. F., Butler, J. H., and Myers, R. C.: Tropospheric SF_6: Observed latitudinal distribution and trends, derived emissions and interhemispheric exchange time, Geophys. Res. Lett., 24, 675–678, doi: 10.1029/97GL00523, 1997. 13655

Glatthor, N., von Clarmann, T., Fischer, H., Funke, B., Gil-López, S., Grabowski, U., Höpfner, M., Kellmann, S., Linden, A., López-Puertas, M., Mengistu Tsidu, G., Milz, M., Steck, T., Stiller, G. P., and Wang, D.-Y.: Retrieval of stratospheric ozone profiles from MIPAS/ENVISAT limb emission spectra: a sensitivity study, Atmos. Chem. Phys., 6, 2767–2781, 2006, http://www.atmos-chem-phys.net/6/2767/2006/. 13659

Hall, T. M. and Waugh, D. W.: Influence of nonlocal chemistry on tracer distributions: Inferring the mean age of air from SF_6, J. Geophys. Res., 103, 13,327–13,336, doi:10.1029/98JD00170, 1998. 13669

Hauchecorne, A., Bertaux, J.-L., Dalaudier, F., Russell III, J. M., Mlynczak, M. G., Kyrölä, E., and Fussen, D.: Large increase of NO_2 in the north polar mesosphere in January-February 2004: Evidence of a dynamical origin from GOMOS/ENVISAT and SABER/TIMED data, Geophys. Res. Lett., 34, L03810, doi:10.1029/2006GL027628, 2007. 13668

Höpfner, M., Oelhaf, H., Wetzel, G., Friedl-Vallon, F., Kleinert, A., Lengel, A., Maucher, G., Nordmeyer, H., Glatthor, N., Stiller, G. P., von Clarmann, T., Fischer, H., Kröger, C., and Deshler, T.: Evidence of scattering of tropospheric radiation by PSCs in mid–IR limb emission spectra: MIPAS–B observations and KOPRA simulations, Geophys. Res. Lett., 29, 1278, doi: 10.1029/2001GL014443, 2002. 13659

Kida, H.: General circulation of air parcels and transport characteristics derived from a hemispheric GCM, Part 2, Very long-term motions of air parcels in the troposphere and stratosphere, J. Meteorol. Soc. Jpn., 61, 510–522, 1983. 13655

Ko, M. K. W., Sze, N. D., Wang, W.-C., Shia, G., Goldman, A., Murcray, F. J., Murcray, D. G., and Rinsland, C. P.: Atmospheric sulfur hexafluoride: Sources, sinks and greenhouse warming,

J. Geophys. Res., 98, 10,499–10,507, doi:10.1029/93JD00228, 1993. 13655

Konopka, P., Engel, A., Funke, B., Müller, R., Grooß, J.-U., Günther, G., Wetter, T., Stiller, G. P., von Clarmann, T., Glatthor, N., Oelhaf, H., Wetzel, G., López-Puertas, M., Pirre, M., Huret, N., and Riese, M.: Ozone loss driven by nitrogen oxides and triggered by stratospheric warmings can outweigh the effect of halogens, J. Geophys. Res., 112, D05105, doi:10.1029/2006JD007064, 2007. 13668

López-Puertas, M. and Taylor, F. W.: Non-LTE radiative transfer in the Atmosphere, World Scientific Pub., Singapore, 2001. 13659

Manney, G. L., Krüger, K., Sabutis, J. L., Sena, S. A., and Pawson, S.: The remarkable 2003–2004 winter and other recent warm winters in the Arctic stratosphere since the late 1990s, J. Geophys. Res., 110, D04107, doi:10.1029/2004JD005367, 2005a. 13668

Manney, G. L., Sabutis, J. L., Allen, D. R., Lahoz, W. A., Scaife, A. A., Randall, C. E., Pawson, S., Naujokat, B., and Swinbank, R.: Simulations of Dynamics and Transport During the September 2002 Antarctic Major Warming, J. Atmos. Sci., 62, 690–707, 2005b. 13666, 13667

Morris, R. A., Miller, T. M., Viggiano, A., and Paulson, J. F.: Effects of electron and ion reactions on atmospheric lifetimes of fully fluorinated compounds, J. Geophys. Res., 100, 1287–1294, doi:10.1029/94JD02399, 1995. 13655

Nemtchinov, V. and Varanasi, P.: Thermal infrared absorption cross-sections of CF_4 for atmospheric applications, J. Quant. Spectrosc. Radiat. Transfer, 82, 461–471, doi:10.1016/S0022-4073(03)00170-5, 2003. 13661

Nett, H., Carli, B., Carlotti, M., Dudhia, A., Fischer, H., Flaud, J.-M., Perron, G., Raspollini, P., and Ridolfi, M.: MIPAS Ground Processor and Data Products, in: Proc. IEEE 1999 International Geoscience and Remote Sensing Symposium, 28 June – 2 July 1999, Hamburg, Germany, pp. 1692–1696, 1999. 13657

Norton, H. and Beer, R.: New apodizing functions for Fourier spectrometry, J. Opt. Soc. Am, 66, 259–264, (Errata J. Opt. Soc. Am., 67, 419,1977), 1976. 13657

Randall, C. E., Harvey, V. L., Singleton, C. S., Bernath, P. F., Boone, C. D., and Kozyra, J. U.: Enhanced NO_x in 2006 linked to strong upper stratospheric Arctic vortex, Geophys. Res. Lett., 22, L18811, doi:10.1029/2006GL027160, 2006. 13668

Randall, C. E., Harvey, V. L., Singleton, C. S., Bailey, S. M., Bernath, P. F., Codrescu, M., Nakajima, H., and Russell III, J. M.: Energetic particle precipitation effects on the Southern Hemisphere stratosphere in 1992-2005, J. Geophys. Res., 112, D08308, doi:

10.1029/2006JD007696, 2007. 13667

Ravishankara, A. R., Solomon, S., Turnipseed, A. A., and Warren, R. F.: Atmospheric lifetimes of long-lived halogenated species, Science, 259, 194–199, doi:10.1126/science.259.5092.194, 1993. 13655

Ray, E. A., Moore, F. L., Elkins, J. W., Dutton, G. S., Fahey, D. W., Vömel, H., Oltmans, S. J., and Rosenlof, K. H.: Transport into the Northern Hemisphere lowermost stratosphere revealed by in situ tracer measurements, J. Geophys. Res., 104, 26,565–26,580, doi:10.1029/1999JD900323, 1999. 13656

Ray, E. A., Moore, F. L., Elkins, J. W., Hurst, D. F., Romashkin, P. A., S.Dutton, G., and Fahey, D. W.: Descent and mixing in the 1999–2000 northern polar vortex inferred from in situ tracer measurements, J. Geophys. Res., 107, 8285, doi:10.1029/2001JD000961, 2002. 13656

Reddmann, T., Ruhnke, R., and Kouker, W.: Three–dimensional model simulations of SF_6 with mesospheric chemistry, J. Geophys. Res., 106, 14,525–14,537, doi:10.1029/2000JD900700, 2001. 13655, 13669

Rinsland, C. P., Brown, L. R., and Farmer, C. B.: Infrared spectroscopic detection of sulfur hexafluoride (SF_6) in the lower stratosphere and upper troposphere, J. Geophys. Res., 95, 5577–5585, doi:10.1029/89JD03413, 1990. 13656, 13658

Rinsland, C. P., Gunson, M. R., Abrams, M. C., Lowes, L. L., Zander, R., and Mahieu, E.: ATMOS/ATLAS1 measurements of sulfur hexafluoride (SF_6) in the lower stratosphere and upper troposphere, J. Geophys. Res., 98, 20,491–20,494, doi:10.1029/93JD02258, 1993. 13656

Rinsland, C. P., Goldman, A., Stephen, T. M., Chiou, L. S., Mahieu, E., and Zander, R.: SF_6 ground-based infrared solar absorption measurements: long-term trend, pollution events, and a search for SF_5CF_3 absorption, J. Quant. Spectrosc. Radiat. Transfer, 78, 41–53, 2003. 13656

Rinsland, C. P., Boone, C., Nassar, R., Walker, K., Bernath, P., Mahieu, E., Zander, R., McConnell, J. C., and Chiou, L.: Trends of HF, HCl, CCl_2F_2, CCl_3F, $CHCLF_2$ (HCFC-22), and SF_6 in the lower stratosphere from Atmospheric Chemistry Experiment (ACE) and Atmospheric Trace Molecule Spectroscopy (ATMOS) measurements near 30^oN latitude, Geophys. Res. Lett., 32, L16S03, doi:10.1029/2005GL022415, 2005. 13656

Rodgers, C. D.: Inverse Methods for Atmospheric Sounding: Theory and Practice, vol. 2 of Series on Atmospheric, Oceanic and Planetary Physics, edited by: F. W. Taylor,, World Scientific, 2000. 13660, 13661

Rothman, L. S., Jacquemart, D., Barbe, A., Benner, D. C., Birk, M., Brown, L. R., Carleer, M. R., Chackerian Jr., C., Chance, K., Coudert, L. H., Dana, V., Devi, V. M., Flaud, J.-M., Gamache, R. R., Goldman, A., Hartmann, J.-M., Jucks, K. W., Maki, A. G., Mandin, J.-Y., Massie, S. T., Orphal, J., Perrin, A., Rinsland, C. P., Smith, M. A. H., Tennyson, J., Tolchenov, R. N., Toth, R. A., Vander Auwera, J., Varanasi, P., and Wagner, G.: The *HITRAN* 2004 molecular spectroscopic database, J. Quant. Spectrosc. Radiat. Transfer, 96, 139–204, doi: 10.1016/j.jqsrt.2004.10.008, 2005. 13658

Schmidt, U. and Khedim, A.: In situ measurements of carbon dioxide in the winter Arctic vortex and at midlatitudes: An indicator of the "age" of stratospheric air, Geophys. Res. Lett., 18, 767–766, 1991. 13669

Seppälä, A., Verronen, P. T., Clilverd, M. A., Randall, C. E., Tamminen, J., Sofieva, V., Backman, L., and Kyrölä, E.: Arctic and Antarctic polar winter NO_x and energetic particle precipitation in 2002-2006, Geophys. Res. Lett., 34, L12810, doi:10.1029/2007GL029733, 2007. 13668

Spang, R., Remedios, J. J., and Barkley, M. P.: Colour indices for the detection and differentiation of cloud types in infra–red limb emission spectra, Adv. Space Res., 3, 1041–1047, doi:10.1016/S0273-1177(03)00585-4, 2004. 13659

Steck, T.: Methods for determining regularization for atmospheric retrieval problems, Appl. Opt., 41, 1788–1797, 2002. 13660

Steck, T. and von Clarmann, T.: Constrained profile retrieval applied to the observation mode of the Michelson Interferometer for Passive Atmospheric Sounding, Appl. Opt., 40, 3559–3571, 2001. 13660

Stiller, G. P., von Clarmann, T., Funke, B., Glatthor, N., Hase, F., Höpfner, M., and Linden, A.: Sensitivity of trace gas abundances retrievals from infrared limb emission spectra to simplifying approximations in radiative transfer modelling, J. Quant. Spectrosc. Radiat. Transfer, 72, 249–280, 2002. 13658, 13662

Strunk, M., Engel, A., Schmidt, U., Volk, C. M., Wetter, T., Levin, I., and Glatzel-Mattheier, H.: CO_2 and SF_6 as stratospheric age tracers: consistency and the effect of mesospheric SF_6–loss, Geophys. Res. Lett., 27, 341–344, doi:10.1029/1999GL011044, 2000. 13656

Tikhonov, A.: On the solution of incorrectly stated problems and method of regularization, Dokl. Akad. Nauk. SSSR, 151, 501–504, 1963. 13660

Varanasi, P., Li, Z., Nemtchinov, V., and Cherukuri, A.: Spectral Absorption–Coefficient Data on HCFC–22 and SF_6 for Remote–Sensing Applications, J. Quant. Spectrosc. Radiat. Transfer, 52, 323–332, 1994. 13659

ACPD

7, 13653–13697, 2007

Global mean age of air from MIPAS

G. P. Stiller et al.

EGU

Volk, C. M., Elkins, J. W., Fahey, D. W., Dutton, G. S., Gilligan, J. M., Loewenstein, M., Podolske, J. R., Chan, K. R., and Gunson, M. R.: Evaluation of source gas lifetimes from stratospheric observations, J. Geophys. Res., 102, 25,543–25,564, doi:10.1029/97JD02215, 1997. 13656

von Clarmann, T., Ceccherini, S., Doicu, A., Dudhia, A., Funke, B., Grabowski, U., Hilgers, S., Jay, V., Linden, A., López-Puertas, M., Martín-Torres, F.-J., Payne, V., Reburn, J., Ridolfi, M., Schreier, F., Schwarz, G., Siddans, R., and Steck, T.: A blind test retrieval experiment for infrared limb emission spectrometry, J. Geophys. Res., 108, 4746, doi:10.1029/2003JD003835, 2003a. 13658

von Clarmann, T., Glatthor, N., Grabowski, U., Höpfner, M., Kellmann, S., Kiefer, M., Linden, A., Mengistu Tsidu, G., Milz, M., Steck, T., Stiller, G. P., Wang, D. Y., Fischer, H., Funke, B., Gil-López, S., and López-Puertas, M.: Retrieval of temperature and tangent altitude pointing from limb emission spectra recorded from space by the Michelson Interferometer for Passive Atmospheric Sounding (MIPAS), J. Geophys. Res., 108, 4736, doi:10.1029/2003JD003602, 2003b. 13658, 13659, 13673

Waugh, D. W. and Hall, T. M.: Age of stratospheric air: theory, observations, and models, Rev. Geophys., 40, 1010, doi:10.1029/2000RG000101, 2002. 13655, 13656, 13666, 13667, 13669

Waugh, D. W., Strahan, S. E., and Newman, P. A.: Transport and modeling of stratospheric inorganic chlorine, Atmos. Chem. Phys. Discuss., 7, 8597–8616, 2007, http://www.atmos-chem-phys-discuss.net/7/8597/2007/. 13655

Zander, R., Rinsland, C. P., and Demoulin, P.: Infrared spectroscopic measurements of the vertical column abundance of sulfur hexafluoride, SF_6, from the ground, J. Geophys. Res., 96, 15 447–15 454, doi:10.1029/91JD01214, 1991. 13656

Zander, R., Gunson, M. R., Farmer, C. B., Rinsland, C. P., Irion, F. W., and Mahieu, E.: The 1985 chlorine and fluorine inventories in the stratosphere based on ATMOS observations at 30° North latitude, J. Atm. Chem., 15, 171–186, doi:10.1007/BF00053758, 1992. 13656

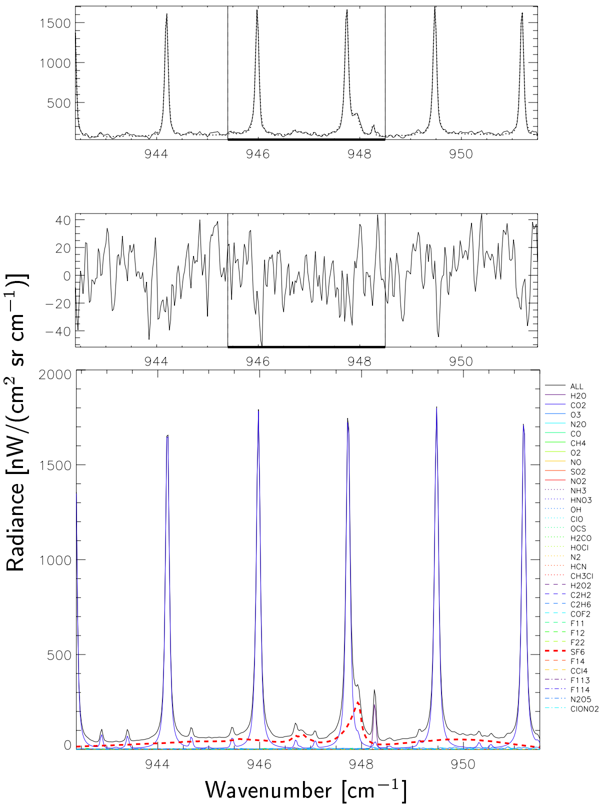

Fig. 1. Typical MIPAS spectrum (measured on 5 November 2003 at 12 km tangent altitude) (top), residual differences between measurement and best-fit spectrum (middle), and trace species spectral contributions (bottom). The bold horizontal line together with the vertical lines in the top two panels indicate the spectral range used within the retrievals. Main contributors are SF_6 (bold dashed red), CO_2 FB laser band (blue, large spectral lines) and CO_2 FH laser band lines (blue, small spectral lines), and water vapour (violet).

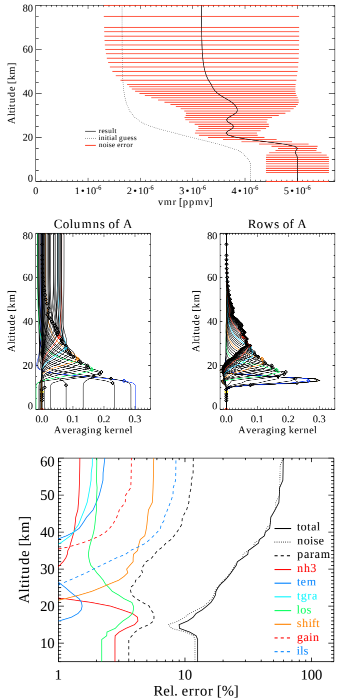

Fig. 2. Typical profile (top), columns and rows of the averaging kernel (middle), and relative error budget (in percent) (bottom), for a measurement of 5 November 2003. All spectra below 12.7 km have been excluded from the retrieval because of cloud contamination (cloud index less than or equal to 6). Error sources assessed are measurement noise (noise),the uncertainties in temperature (tem), line-of-sight (los) (from preceding retrievals), NH_3 (nh3)(from climatological variability), and horizontal temperature gradients (tgra), residual uncertainties in radiometric (gain) and frequency shift calibration (shift), and residual uncertainties in the instrumental line shape (ils). The quadratic sum of all errors except measurement noise is given by the black dashed line (param), while the quadratic sum over all error sources is given by the black solid line (total).

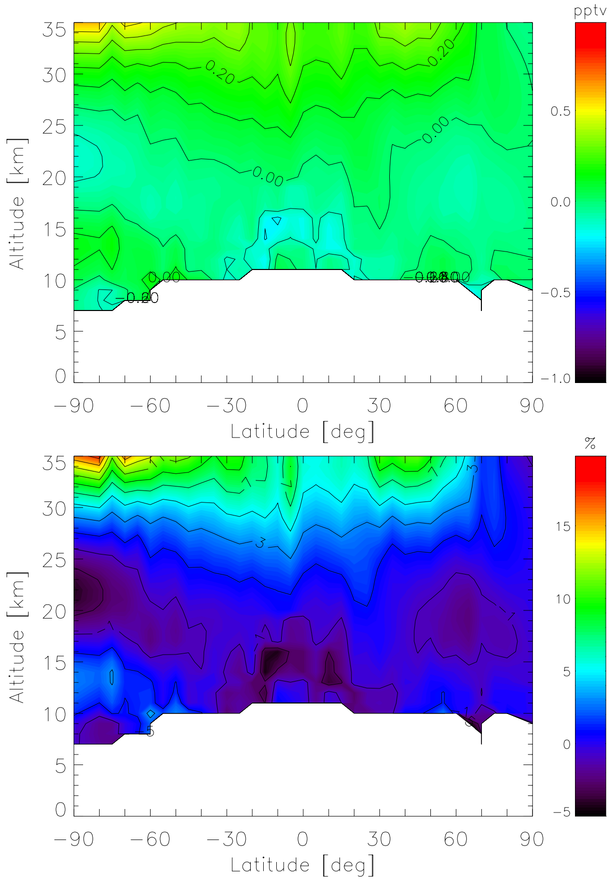

Fig. 3. Mean differences of profiles (top: absolute in pptv, bottom: relative in percent) between the retrieval which fully considers CO_2 non-LTE emissions and the standard retrieval (non-LTE - standard) for 1 January 2004. The 5° latitudinal mean differences for a full day of observations (1000 scans in total distributed within 35 latitude bands) are shown. White areas are missing data due to clouds.

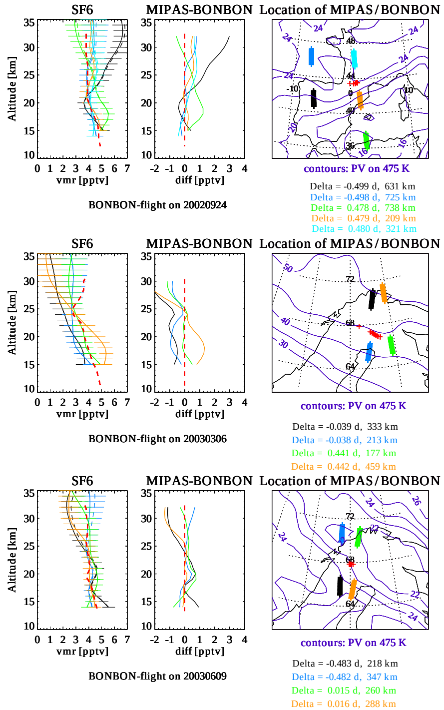

Fig. 4. Comparison of individual SF_6 profiles with co-located in situ observations obtained during balloon flights of a cryogenic whole-air sampler (BONBON) (Engel et al., 2006b), for (top) 24 September 2002 over Southern France, and (middle) 6 March 2003 and (bottom) 9 June 2003 over Northern Scandinavia. The left panels show the profiles measured by MIPAS (colours except red) and BONBON (red) for the best co-incidences. The middle panels provide the difference profiles between MIPAS and BONBON. In the right panels the location of the observations are shown together with the PV contours on 475 K (violet contour lines, PV units: K m^2 kg^{-1} s^{-1}) and the temporal and spatial distances. For the September 2002 flight, in addition the bias-corrected MIPAS observations are given (dashed coloured lines except red in the left panel).

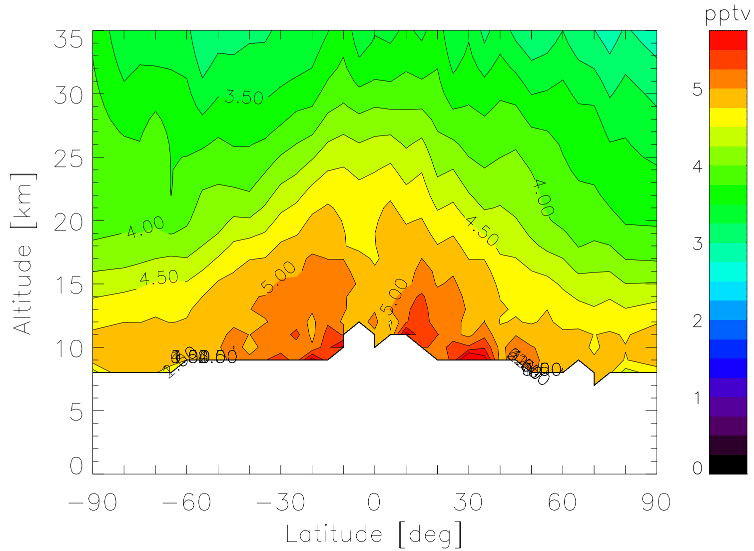

Fig. 5. Global mean distribution of SF_6 (bias-corrected) for March 2003 (geographical latitude versus altitude, 5° latitude bins; approximately 140 profiles per latitude bin). White areas are missing data due to clouds.

ACPD

7, 13653–13697, 2007

Global mean age of air from MIPAS

G. P. Stiller et al.

EGU

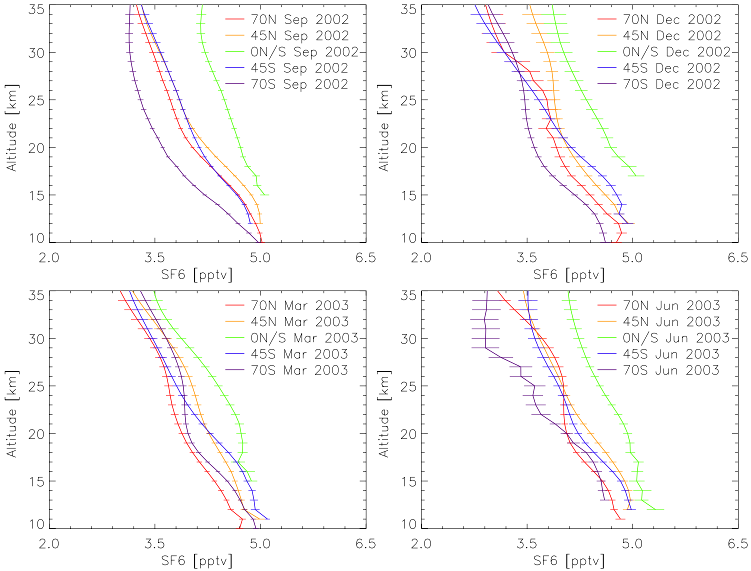

Fig. 6. Seasonal and latitudinal variability of SF_6 profiles: The lines represent zonal (5° latitude bins) monthly means from 100–150 single profiles for the months September 2002, December 2002, March 2003, and June 2003, and for the latitudes 70° N, 45° N, 0°, 45° S, and 70° S. Error bars represent the 1σ standard errors of the mean.

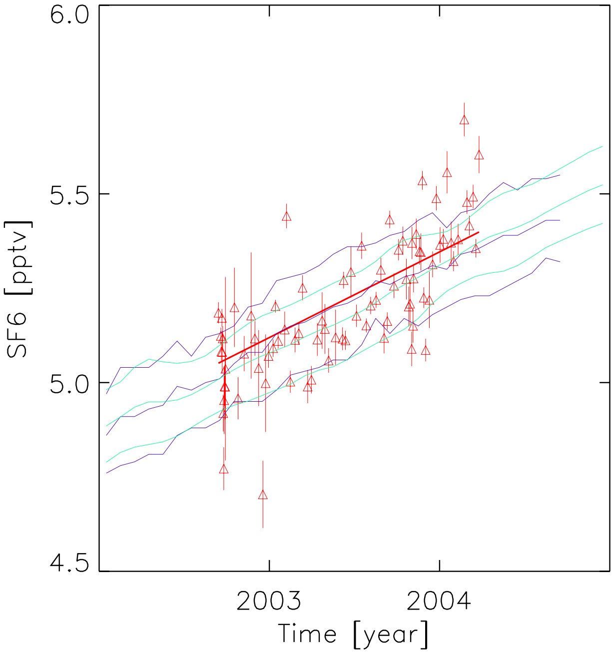

Fig. 7. Tropical tropospheric trend derived from the daily bias-corrected zonal mean distributions of SF_6 within 17.5° N and 17.5° S and 9 to 15 km altitude (red symbols and red solid line; error bars are the 1σ standard errors of the daily means). Time series of NOAA/ESRL/GMD flask measurements (violet) and in situ measurements (green) for the Northern hemisphere (highest lines), global mean (middle lines), and Southern hemisphere (lowest lines) are also shown. The trend derived from MIPAS measurements is 0.227±0.008 pptv yr^{-1}.

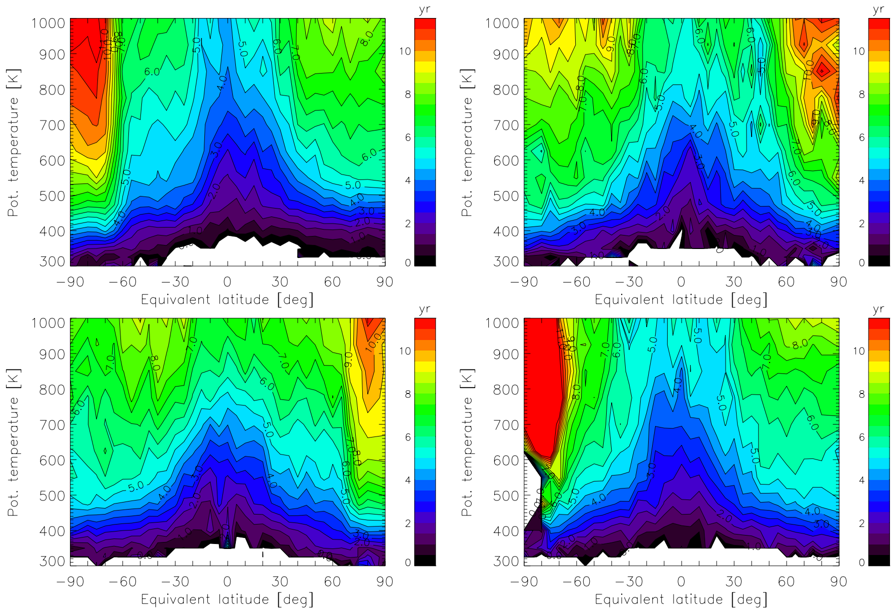

Fig. 8. Global distributions of mean age of stratospheric air (potential temperature versus equivalent latitudes) for the months September 2002 (top left), December 2002 (top right), March 2003 (bottom left), and June 2003 (bottom right).

ACPD

7, 13653–13697, 2007

EGU

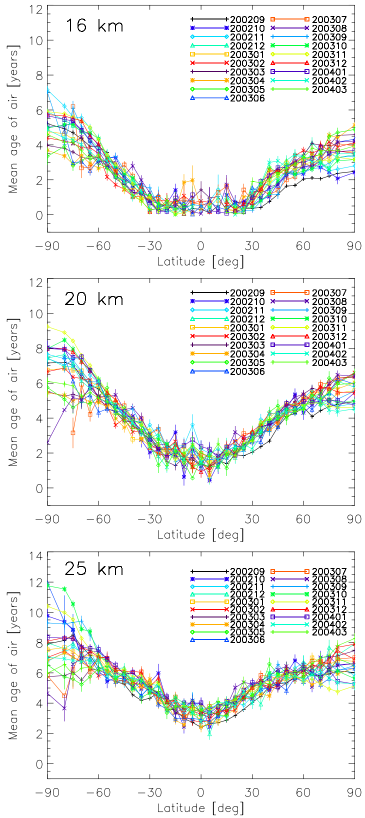

Fig. 9. Mean age of air at (top) 16 km, (middle) 20 km, and (bottom) 25 km altitude from MIPAS/Envisat SF_6 distributions; presented are the monthly zonal means for 5°latitude bins for all months between September 2002 and March 2004. The error bars represent the 1σ standard errors of the mean.

ACPD

7, 13653–13697, 2007

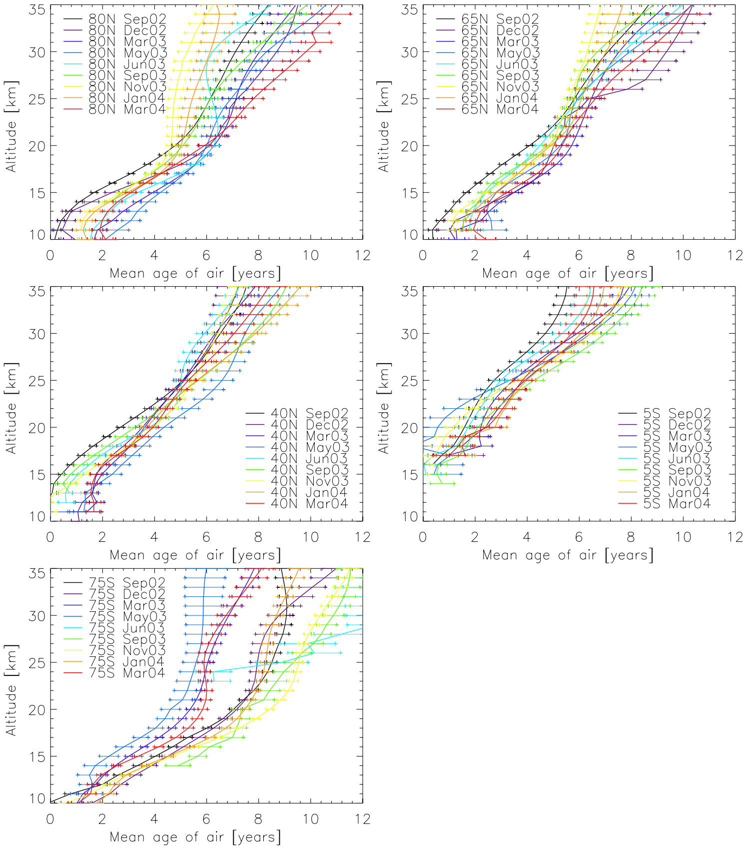

Fig. 10. Monthly zonal mean age of stratospheric air profiles for 80° N, 65° N, 40°N, 5°S, and 75° S for the months September 2002 (black), December 2002 (violet), March 2003 (dark blue), May 2003 (light blue), June 2003 (turquoise), September 2003 (green), November 2003 (yellow), January 2004 (orange), and March 2004 (red). Errors represent the 1σ standard errors of the mean (horizontal lines).

ACPD

7, 13653–13697, 2007

EGU

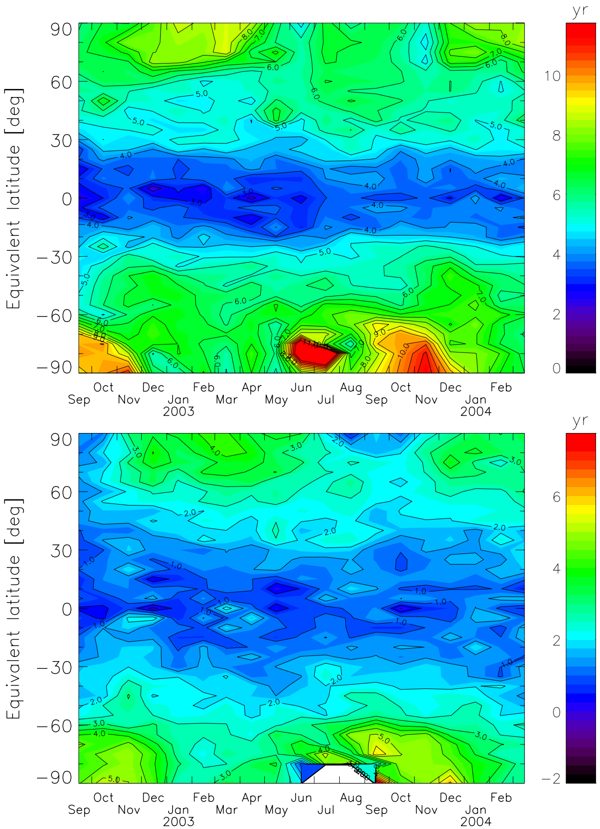

Fig. 11. Global time series of zonal distributions of the mean age of stratospheric air at the 625 K (top) and 400 K (bottom) level (versus equivalent latitude), constructed from monthly means. Note the different colour scales in the two panels. The white area in the 400 K panel is due to missing data due to clouds (PSCs).

ACPD
7, 13653–13697, 2007

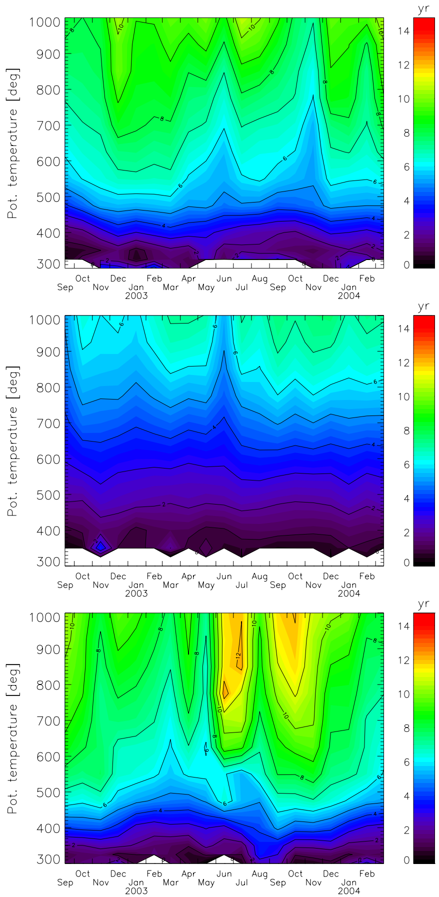

Fig. 12. Time series of mean age of stratospheric air vertical profiles (constructed from monthly zonal means) (potential temperature as vertical coordinates) for the equivalent latitude bands 60° N–90° N (top), 20°S–20° N (middle), and 90° S–60° S (bottom).

ACPD

7, 13653–13697, 2007

Global mean age of air from MIPAS

G. P. Stiller et al.

EGU

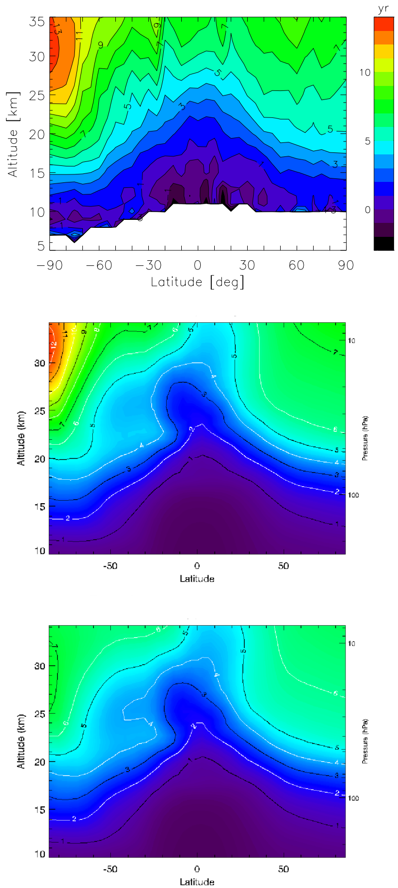

Fig. 13. Zonal mean distribution of mean age of stratospheric air for October 2003 from MIPAS (top), and KASIMA with (middle) and without (bottom) consideration of the SF_6 loss reaction in the mesosphere, giving the apparent and the true mean age, respectively.

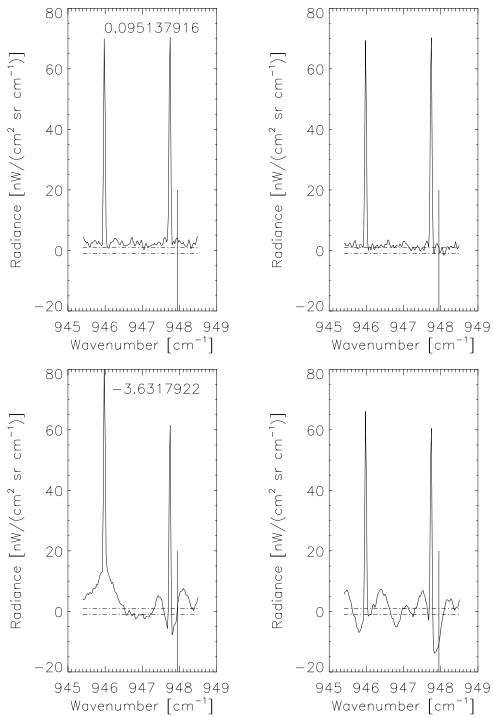

Fig. 14. Averaged radiance spectra of the highest tangent altitudes (i.e. approximately 68 km) in the region of the SF_6 signature for an example of close-to-perfect (top) and heavily distorted radiance calibration (bottom), respectively. The spectra were averaged over the period when one specific gain calibration function was applied; this is 8 to 9 December 2002 for the top panel and 28 to 30 April 2003 for the bottom panel. Averaging was done for forward (left) and backward (right) sweeps separately. The horizontal dashed lines indicate the expected NESR for the averaged spectra. The vertical solid line gives the position of the SF_6 peak. The number provides the value of the gain index derived (for further details see text).

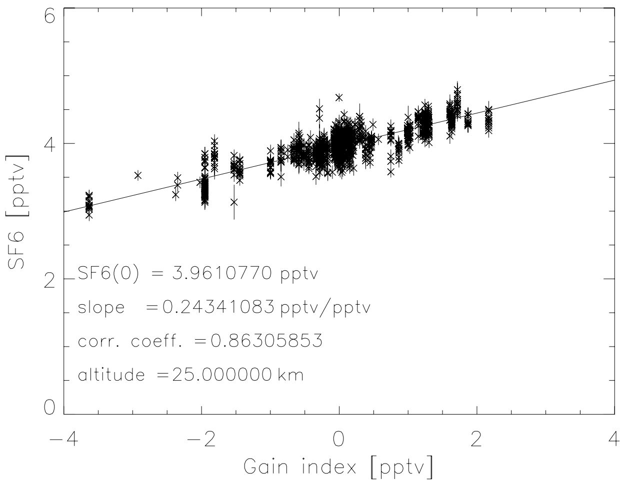

Fig. 15. Correlation between orbit-averaged SF_6 vmrs and orbit-related gain indices for the altitude level 25 km. The vertical lines are the standard errors of the orbit means. The text provides the abscissa [pptv] (top), slope (second line), correlation coefficient (third line), and altitude [km] (fourth line).

ACPD
7, 13653–13697, 2007

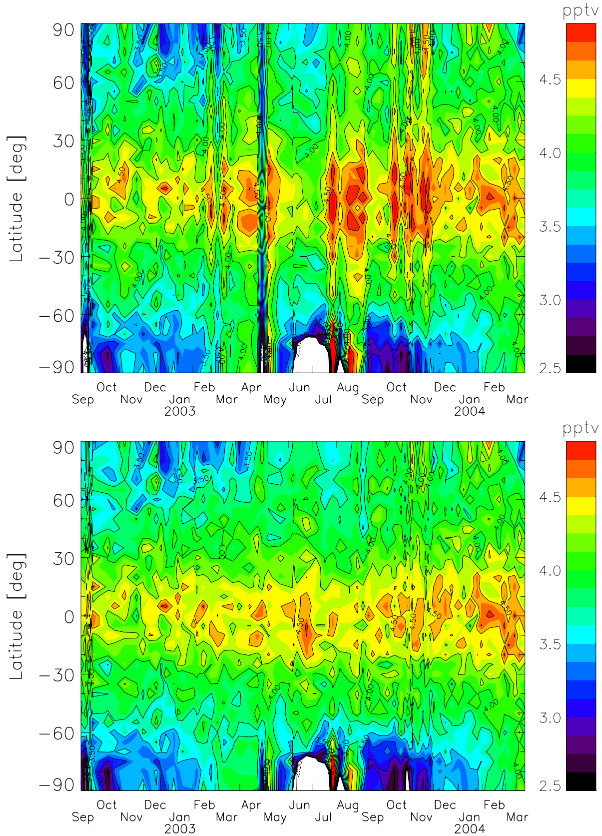

Fig. 16. Time series of SF_6 zonal mean distributions at 25 km altitude before (top) and after (bottom) correction for the bias due to inadequate radiance calibration. Remnants of the gain-calibration caused artefacts remained for some days and regions, particularly for high Southern latitudes on 29 April 2003, 7 May 2003, and 27 July 2003, and for high Northern latitudes for some days during November 2003. White areas indicate SF_6 values below 2.5 pptv or missing data due to clouds (PSCs).

ACPD
7, 13653–13697, 2007

Global mean age of air from MIPAS

G. P. Stiller et al.

EGU